Dynamic changes in 1H-MR relaxometric properties of cell-internalized paramagnetic liposomes, as studied over a properties of cell-internalized paramagnetic liposomes, as studied over a five-day period

CONTRAST MEDIA & MOLECULAR IMAGING

Received: 2 April 2010, Revised: 20 June 2010, Accepted: 24 June 2010, Published online in Wiley Online Library: 9 October 2010

(wileyonlinelibrary.com) DOI:10.1002/cmmi.406

Dynamic changes in ^{1}H-MR relaxometric properties of cell-internalized paramagnetic liposomes, as studied over a five-day period

Maarten B. Kok[a], Gustav J. Strijkers[a] and Klaas Nicolay[a]*

Molecular imaging based on MRI requires the use of amplification strategies in order to achieve sufficient sensitivity for the detection of low-level molecular markers. Recently, we described a combination of two amplification methods: (i) the use of paramagnetic liposomes that can be prepared with a high payload of Gd^{3+}-containing lipid; and (ii) targeting to a cell-surface receptor that can undergo multiple rounds of nanoparticle delivery in the cell, followed by recycling to the cell membrane. Liposome uptake was monitored over a period of 24 h and was found to lead to massive delivery in subcellular compartments. The present study aimed to monitor the longer-term fate of the cell-internalized contrast material by studying its relaxometric properties over 5 days, following an initial 24 h loading period. Circa 25% of the Gd^{3+}-content delivered to the cells via integrin-targeted liposomes was lost in the first 24 h, which led to 65 and 77% reductions in R_1 and R_2, respectively, as compared with the original R_1 and R_2 enhancements. This implies that the remaining cell-associated gadolinium had relatively low effective r_1 and r_2 relaxivities. It is proposed that this is due to gradual release of Gd^{3+} from the chelate in the cell, followed by sequestration in an MR silent state. Most of the gadolinium internalized by cells following incubation with non-targeted liposomes was released in the 5-day follow-up period. Copyright © 2010 John Wiley & Sons, Ltd.

Keywords: MRI; liposomes; RGD; HUVEC; relaxivity; internalization; release

1. INTRODUCTION

In recent years, a lot of progress has been made in the development of molecular imaging technologies for the *in vivo* visualization of specific markers of biological processes, both under normal and pathological conditions (1). Molecular imaging is expected to greatly impact both basic and translational medicine, as it strongly enhances both the specificity and the sensitivity of imaging-based disease detection and monitoring. Among the major imaging modalities, PET and SPECT have traditionally played a leading role in the development of molecular imaging tools for the clinic, while the abilities of MRI-based molecular imaging until recently have remained largely unexplored. This disparity is mainly due to the large differences in intrinsic detection sensitivity between these techniques. PET and SPECT require minimal contrast agent concentrations between 10^{-12} and 10^{-10} M (2), while the detection threshold for MRI rather is in the order of 10^{-5} to 10^{-4} M (3). However, in view of the extraordinary versatility of MRI for providing non-invasive anatomical, functional as well as metabolic read-outs of tissue status, important steps have been taken recently to extend the abilities of MRI to the visualization of molecular and cellular markers.

One prominent approach in molecular MRI is the use of Gd^{3+}-based paramagnetic contrast agents that produce a local shortening of the T_1 relaxation time. The most suitable design of these Gd^{3+}-based agents depends on the specific application, such as the abundance and accessibility of the intended target. Low numbers of Gd^{3+} per contrast agent construct may suffice for high-level targets, while a high Gd payload is typically required for the detection of low-level targets. Nanoparticles can be equipped with many Gd-chelates and therefore are extensively studied for their utility in molecular MRI (3–6). In recent years, we have explored the use of paramagnetic liposomes, a major class of biocompatible nanoparticles that can be prepared in a range of sizes, generally between 50 and 500 nm (4). The liposomes are mainly made from naturally occurring lipids, such as phosphatidylcholine and cholesterol, and therefore their prime constituents are biocompatible and well suited for biomedical applications. For MRI contrast, we typically include 25 mol% of a non-natural lipid, which contains a Gd-chelate in the polar head group. The Gd-chelate is thus located in the interface between the hydrophobic interior of the liposomal bilayer and the surrounding aqueous medium, ensuring efficient access of bulk water protons to the paramagnetic center. Relaxometric studies of paramagnetic liposomes, equipped with 25 mol% Gd–DTPA-bis(stearylamide) (7), indicated that their relaxivity r_1 should enable the detection of molecular markers in the sub-nanomolar concentration range. Based on these findings, we have recently studied the *in vitro* homing of RGD-conjugated paramagnetic liposomes to cultured endothelial cells over-expressing the $\alpha_v\beta_3$-integrin cell-surface receptor. This RGD–integrin ligand–target couple has been widely studied (8) and therefore is very attractive for investigating critical aspects of target-specific MRI. The prime clinical application of $\alpha_v\beta_3$-integrin imaging is the detection of tumor angiogenesis: activated tumor

* *Correspondence to: K. Nicolay, Biomedical NMR, Department of Biomedical Engineering, Eindhoven University of Technology, PO Box 513, 5600 MB Eindhoven, The Netherlands.*
E-mail: k.nicolay@tue.nl

a *M. B. Kok, G. J. Strijkers, K. Nicolay*
Biomedical NMR, Department of Biomedical Engineering, Eindhoven University of Technology, 5600 MB Eindhoven, The Netherlands

endothelium abundantly expresses the integrin, while quiescent endothelial cells in mature blood vessels only express low levels. The MRI-based visualization of tumor neo-angiogenesis has been pioneered by Sipkins *et al*., who also utilized integrin targeted paramagnetic liposomes (9). Our initial integrin targeting studies involved up to 24 h incubations of human umbilical vein endothelial cells (HUVEC) with RGD-conjugated liposomes, using non-conjugated particles as a control (10). It was found that functional, integrin-targeted liposomes were abundantly taken up by the HUVEC and were mainly localized in intracellular vesicles in the perinuclear region of the cell. The uptake of RGD-liposomes most likely occurred via receptor-mediated endocytosis as the $\alpha_v\beta_3$-integrin is known to be an internalizing receptor (11,12). This is, in principle, an attractive targeting concept: it involves the receptor to recycle back to the cell membrane after cargo delivery, thus enabling amplified delivery of imaging agent to the target cell over-expressing the disease marker. Functional paramagnetic liposomes were taken up by HUVEC in a 15-fold higher amount than their non-functional counterparts (10). Importantly, however, the increase in cellular longitudinal relaxation rate R_1 brought about by integrin-targeted and non-targeted particles differed much less (*ca* 3.7- vs 3.4-fold, respectively). This implies that the effective relaxivity r_1 of the functional liposomes was strongly reduced compared with its intrinsic value. Using mathematical modeling, Strijkers *et al*. (13) provided convincing evidence that this so-called r_1 quenching effect is due to confinement of the paramagnetic material in a low-volume fraction intracellular compartment from which water proton exchange with the bulk is too slow to come to full expression of the intrinsic liposomal r_1. The effects of cell internalization of the liposomes on their r_2 were relatively small and rather indicated a somewhat increased T_2 shortening effect (10). Cytotoxicity assays indicated that the high amounts of cell-internalized liposomes caused minimal cell death over the 24 h incubation period (10).

The purpose of the present study was to examine the relaxometric properties of HUVEC-associated paramagnetic liposomes over a period of 5 days. To this aim, HUVEC were incubated with either $\alpha_v\beta_3$-integrin targeted or non-targeted liposomes for 24 h. After this initial loading period, fresh liposome-free growth medium was supplied and cell samples were collected over a period of 120 h and analyzed using MRI, fluorescent activated cell sorting (FACS), inductively coupled plasma mass spectrometry (ICP-MS) and confocal laser scanning microscopy (CLSM). These experiments provide important insights in the longer-term fate of cell-internalized liposomes and possible changes in their effective T_1- and T_2-shortening capacity. This study is also relevant for MRI-based cell tracking research, in which cells are loaded *in vitro* with paramagnetic contrast agent, followed by *in vivo* implantation and long-term MRI monitoring of cell migration (14–18).

2. RESULTS

The characteristics of cell-internalized paramagnetic, fluorescent liposomes were studied over a period of 5 days. The cellular location of the contrast agent was determined using CLSM, exploiting the fluorescent rhodamine-PE lipid present in the bilayer of the liposomes. The left column of Fig. 1 shows confocal images of HUVEC grown on gelatin-coated coverslips, following 24 h incubations with RGD- or NT-liposomes. CLSM revealed a cobblestone-like structure of the HUVEC, which is characteristic for healthy, confluent endothelial cells. This morphology was observed throughout the entire experiment, for both RGD- and NT-liposome treated cells. For incubations with RGD-liposomes, large rhodamine-PE positive vesicular structures with a diameter of 1–5 μm, were observed throughout the cytoplasm. Incubation with NT-liposomes resulted predominantly in staining of the perinuclear region of the cell and fluorescent signal in this case originated from more sharply defined and smaller (i.e. 0.4–1.0 μm diameter) spherical vesicles. These CLSM data are in line with a previous study (10), except that the higher degree of confluency of the cells resulted in sharper delineation of CD31 positive cell-cell junctions.

In our previous study (10), Lysotracker Green, a marker for acidic intracellular compartments like lysosomes, was used to establish the nature of the vesicular structures that contain the internalized liposomes. It appeared that all rhodamine-PE positive cellular structures were also positive for Lysotracker Green, indicating that the liposomes are taken up into compartments of

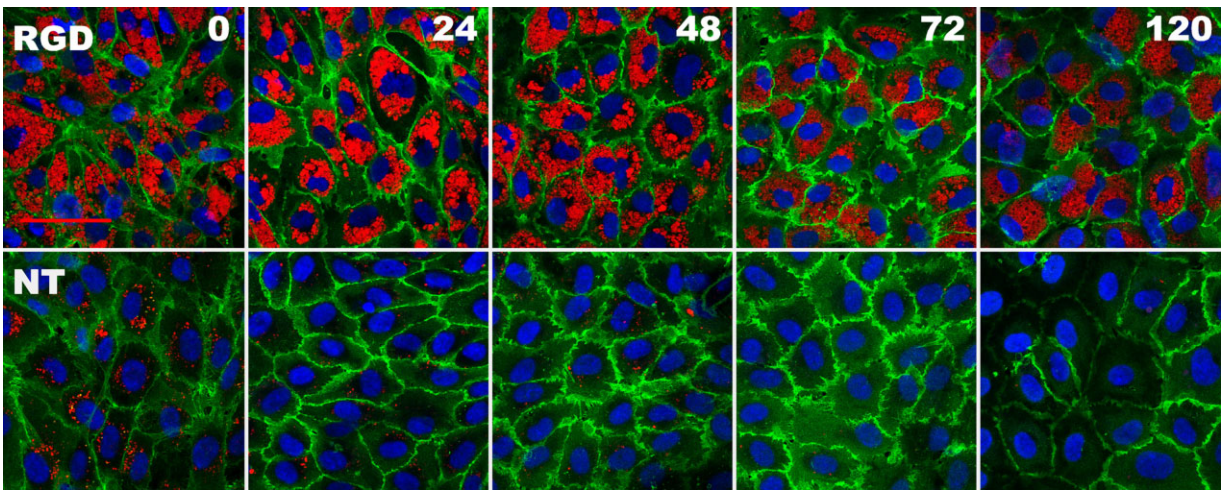

Figure 1. CLSM images of HUVECs after loading of the cells with RGD-liposomes (RGD) or NT-liposomes (NT). The numbers in the top right corner represent the incubation times (in h) with liposome-free medium, after the initial 24 h loading with paramagnetic liposomes. The colors in the fluorescence microscopic images are as follows: blue = DAPI, staining cell nuclei; green = CD31, which stains the plasma membrane of the endothelial cells; red = rhodamine-PE, representing fluorescent signal originating from the liposomes.

the endocytic pathway. In addition, we showed in the same paper that most intracellular structures that were positive for RGD-conjugated liposomes were also $\alpha_v\beta_3$-integrin positive, while non-targeted liposomes were predominantly internalized into integrin-negative vesicles. The latter finding suggests that the functional and non-functional liposomes reside in different intracellular compartments.

Under the present experimental conditions (i.e. following removal of the non-cell associated, extracellular liposomes via extensive washing), no detectable association of liposomes with the cell membrane was observed for both RGD- and NT-liposome incubated HUVEC. This implies that the measured R_1 and R_2 dynamics were dominated by intracellular events and barely affected by agent that was associated with the extracellular surface of the cell.

Following removal of the liposomes after 24 h and continued incubation with fresh medium, over time distinct differences were observed in spatial distribution and intensity of fluorescent signal from HUVEC pre-incubated with RGD- or NT-liposomes. Up to 48 h after initial loading of the HUVECs with RGD-liposomes, the rhodamine signal was located in sharply-defined vesicular structures present throughout the entire cytoplasm. For longer incubation times the vesicular structures became less sharply defined. Also a diffuse cytoplasmic rhodamine signal was observed after 48 h, which intensified up to 120 h of incubation. NT-liposomes showed a different behavior. After loading of the HUVECs, the rhodamine signal mainly originated from small vesicular structures in the perinuclear region of the cell. Over time the number of rhodamine-PE-positive vesicles gradually decreased and very little fluorescence was observed at the 120 h time point.

FACS was used to measure the mean rhodamine-PE fluorescence intensity (MFI) per cell (Fig. 2A, B). MFI data were indicative of a 35-fold higher uptake of RGD-liposomes after 24 h of incubation, compared with NT-liposomes. FACS revealed a 31% reduction in MFI for RGD-liposome treated HUVEC over the first 24 h incubation with liposome-free medium, after which an essentially stable level of cell-associated fluorescence was observed up to the final measurement at 120 h (Fig. 2A). HUVEC incubated with NT-liposomes showed a very different behavior (Fig. 2B). At the 72 h time point, the MFI was reduced by *ca* 85% after which no further decrease occurred.

ICP-MS was used to quantify Gd levels in loosely packed pellets of HUVEC (Fig. 2C, D), which were prepared for quantitative relaxometric MRI measurements. The initial 24 h loading with RGD-liposomes resulted in a concentration of 2.46 ± 0.14 mM Gd in the cell pellet (Fig. 2C). Following 24 h incubation with fresh medium, the cellular Gd level had reduced to 1.96 ± 0.03 mM, while a further minor decrease to 1.84 ± 0.06 mM was noted at the 120 h time point. The latter value represents a 25% drop in Gd levels over 120 h. Pre-incubation with NT-liposomes resulted in an initial gadolinium concentration of 0.20 ± 0.01 mM (Fig. 2D), which decreased to a value of 0.06 ± 0.01 mM after 120 h of incubation with contrast agent-free medium, corresponding to a 71% reduction in cell-associated Gd. Most of the Gd loss from HUVEC incubated with NT-liposomes occurred in the first 24 h.

The results of quantitative T_1 and T_2 measurements on loosely packed pellets of HUVEC are depicted in Figs 3 and 4. Figure 3 shows the relationship between the longitudinal relaxation rate R_1, as measured by MRI at 6.3 T, and the concentration of Gd, as quantified by ICP-MS. The R_1 data are presented as a function of Gd levels (rather than incubation time) to enable a more straightforward estimation of the effective ionic relaxivity r_1 (see Discussion). The R_1 of HUVEC incubated with RGD-liposomes declined from an initial value of $1.78 \pm 0.11\ s^{-1}$ to a final value of $0.93 \pm 0.10\ s^{-1}$ after 120 h. Over the same 120 h period, the R_1 of HUVEC pre-incubated for 24 h with NT-liposomes dropped from

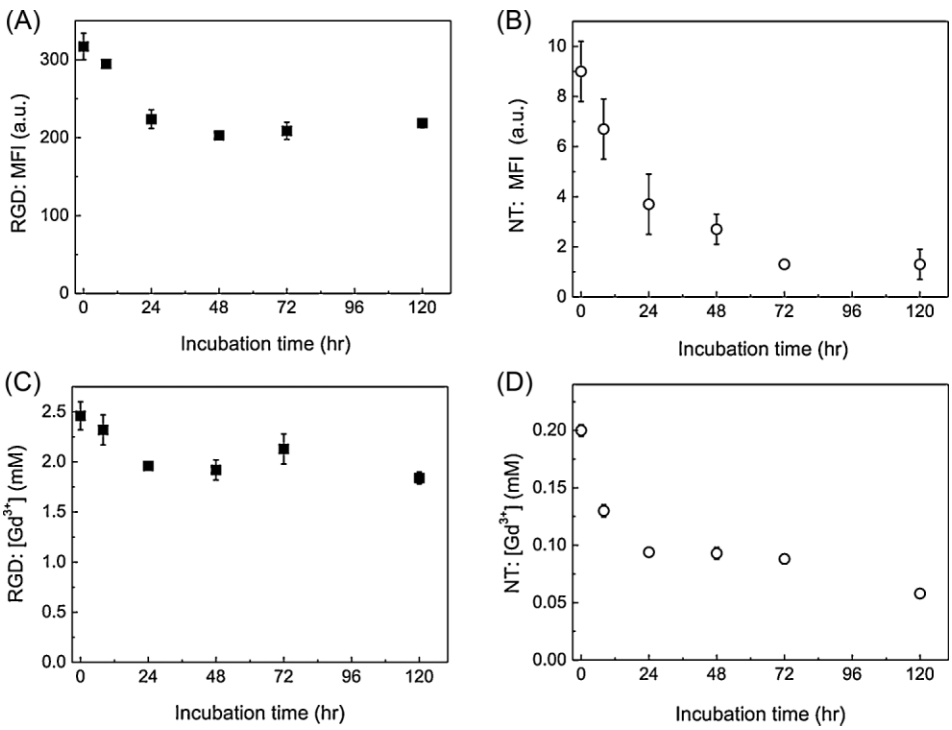

Figure 2. Mean fluorescence intensity (MFI) per cell (A, B) and the cellular gadolinium concentration (C, D) as a function of incubation time for RGD-liposomes (solid squares) and NT-liposomes (open circles). MFI was normalized to the MFI of control cells. Note that the *y*-axis scales differ for RGD- and NT-liposomes. Data represent mean ± SD ($n = 3$).

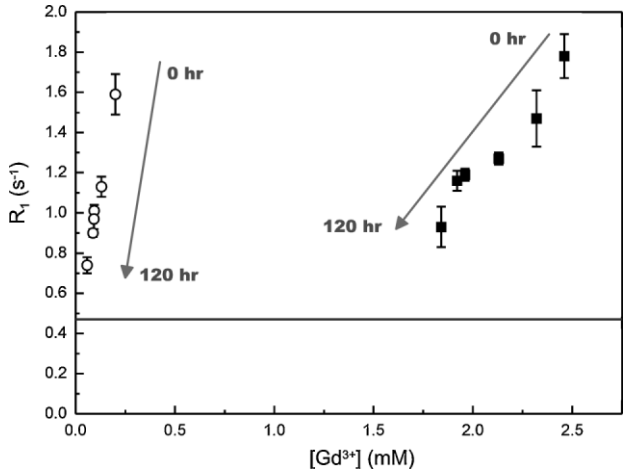

Figure 3. R_1 vs gadolinium concentration of loosely-packed pellets of HUVEC. Longitudinal relaxation rates (R_1) were measured at 6.3 T. Solid squares: HUVEC pre-incubated with RGD-liposomes; open circles: HUVEC pre-incubated with NT-liposomes, in both cases followed by incubation with liposome-free medium. Data represent mean ± SD ($n = 3$). The arrows indicate the prolongation of incubation times. The solid line is the R_1 value measured for control HUVECs.

1.59 ± 0.10 to $0.74 \pm 0.04\ s^{-1}$ (Fig. 3). It should be noted that the R_1 of control HUVEC prior to incubation with paramagnetic liposomes was $0.47 \pm 0.02\ s^{-1}$ at 6.3 T, as averaged from measurements of control HUVEC at each time point. These data imply that the increases in cellular R_1, originally brought about by incubations with RGD- and NT-liposomes, were reduced by 65 and 76%, respectively, at the 120 h time point.

Similar measurements on the influence of prolonged HUVEC incubations in liposome-free growth medium on the transverse relaxation rate R_2 are shown in Fig. 4. R_2 values of HUVEC pre-loaded with RGD-liposomes were reduced from 115.1 ± 6.2 to $50.0 \pm 6.5\ s^{-1}$ over 120 h. For the case of NT-liposomes, the transverse relaxation rates dropped from 34.3 ± 1.6 to $32.1 \pm 0.9\ s^{-1}$, closely approaching the R_2 of control HUVEC ($30.4 \pm 1.4\ s^{-1}$). The data correspond to R_2 reductions of 77 and 57%

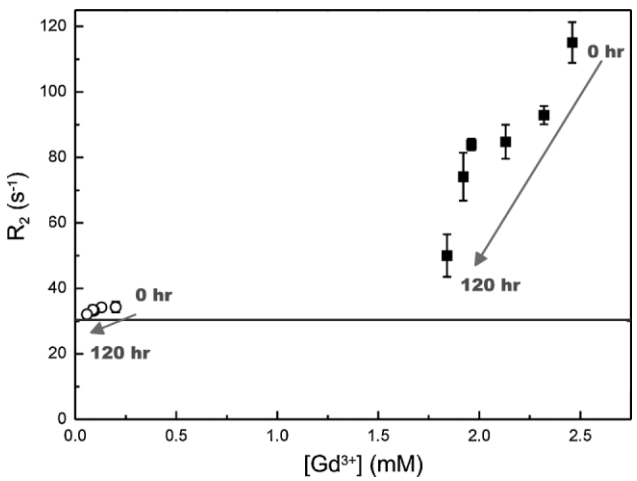

Figure 4. R_2 as a function of concentration of gadolinium in cell pellets for RGD-liposome (solid squares) and NT-liposome (open circles) incubated HUVECs. Data represent mean ± SD ($n = 3$). The arrows indicate the prolongation of incubation times. The solid line is the R_2 value measured for control HUVECs.

compared with the original R_2 enhancements for the case of RGD- and NT-liposomes, respectively.

3. DISCUSSION AND CONCLUSION

The primary aim of the present study was to measure the relaxometric properties of cell-internalized targeted liposomal contrast agents over a period of 5 days. Relaxometry was supported by FACS and fluorescence microscopy, both of which made use of liposomal rhodamine-PE. In line with our earlier study (10), RGD-conjugated liposomes were massively internalized by HUVEC. The absolute level of Gd incorporation was slightly lower as compared with previous experiments, which possibly is due to the high cell confluency. This was close to 100%, compared with 80–90% before and may have led to a more quiescent state of the HUVEC and, consequently, lower levels of $\alpha_v\beta_3$-integrin expression and lower rates of endocytosis. The non-targeted liposomes were taken up to low levels, as before (10).

The key findings of the experiments with integrin-targeted RGD-liposomes are that over the 5-day follow-up period a moderate reduction in the levels of HUVEC-associated Gd (i.e. 25%; Fig. 2C) caused a strong decrease in cellular R_1 enhancement (i.e. 65%; Fig. 3). The latter number was calculated by taking the R_1 of non-liposome incubated HUVEC as a reference. From the RGD-liposome data in Fig. 3, we estimated that the effective relaxivity r_1 of the Gd pool, which was released from the cells over 120 h, amounted to *ca* $1.16 \pm 0.15\ mM^{-1}\ s^{-1}$. This r_1 estimation assumed a linear relationship between R_1 and Gd concentration. The R^2 of the linear fit was 0.93. A very different picture emerged, when applying a similar analysis to the NT-liposome data. Figure 2D demonstrates that 71% of the Gd was released from the cells over 5 days in this case. Interestingly, the data in Fig. 3 reveal that the original R_1 increase compared with control HUVEC was reduced in a similar proportion, i.e. by 76%, over the same time span. The effective relaxivity r_1 of the released Gd pool was estimated to be *ca* $5.85 \pm 0.32\ mM^{-1}\ s^{-1}$ in case of HUVEC pre-incubated with NT-liposomes (the R^2 was 0.98). Similar estimations of the effective r_2 of Gd lost from the cells over the 120 h time period were applied to the R_2 data depicted in Fig. 4. Linear relationships between r_2 and [Gd] were assumed to hold, in line with the above r_1 analysis. Effective r_2s of 79.9 ± 18.2 and $13.9 \pm 5.0\ mM^{-1}\ s^{-1}$ were estimated for RGD- and NT-liposome data, respectively (R^2 were 0.82 and 0.72, respectively).

It is interesting to compare the above numbers on estimated effective relaxivities r_1 and r_2 for Gd released from the cells over the 5-day observation period to the intrinsic relaxivities of the paramagnetic liposomes that were used in this study. In agreement with our previous findings on the effective r_1 relaxivities of paramagnetic liposomes internalized by HUVEC over a 24 h period (10), the effective r_1 of Gd released from the RGD-liposome treated cells in the present study was lower ($1.2\ mM^{-1}\ s^{-1}$) than the intrinsic r_1 of RGD-liposomes ($2.1\ mM^{-1}\ s^{-1}$), while that of the Gd released from NT-liposome treated cells was considerably higher ($5.9\ mM^{-1}\ s^{-1}$) than that of the NT-liposomes ($2.3\ mM^{-1}\ s^{-1}$) in buffer at 6.3 T (10). The opposite holds true for the comparison of the effective r_2s of released Gd. For RGD-liposomes we found values of $79.2\ mM^{-1}\ s^{-1}$, compared with a value of $17.3\ mM^{-1}\ s^{-1}$ for RGD-liposomes as prepared. The release pattern of NT-liposomes corresponded to an effective r_2 of $17.7\ mM^{-1}\ s^{-1}$, compared with an intrinsic value of $19.6\ mM^{-1}\ s^{-1}$. Clearly, the

interpretations of the present data are limited by the lack of insights in the molecular organization of the Gd-containing structures from which it was released and in which it remained associated with the cells. Nevertheless, when combining the relaxometry data with the fluorescence microscopy data, the following picture emerges. The high local levels of Gd that are concentrated in relatively large intracellular inclusions following 24 h treatment with RGD-liposomes inevitably cause a reduction in r_1 and an elevation in r_2 (13). Not surprisingly, the initial release of Gd from the RGD-liposomes treated cells is also associated with a relatively mild reduction in R_1 and a strong reduction in R_2. Using similar reasoning, the low level of delivery of NT-liposomes to relatively small cellular structures can explain the absence of any r_1 quenching and r_2 elevation effect. The reason for the supranormal effective r_1 of cell-associated NT-liposomes, during both the loading and the release phases of our study, remains to be clarified. This possibly has to do with a loss of structural integrity of the liposomes leading to an increased T_1-shortening contribution from Gd–lipid in the inner leaflet of the liposomal bilayer [see also Kok *et al.* (10)].

It is tempting to speculate on the relaxometric properties of the Gd remaining associated with the cells at long incubation times following loading with RGD-liposomes. Extrapolation of the R_1 and R_2 data in Figs 3 and 4 to the R_1 and R_2 values of control cell pellets (0.47 and 30.4 s^{-1}, respectively) led to estimated residual Gd concentrations in the cell pellets as high as 1.4 mM in both cases at which both the liposomal T_1 and T_2 shortening effects would be completely silenced. Obviously, the present data do not provide evidence that such extrapolation is justified, as the cells have not been monitored over a sufficiently long time period. However, our data do suggest that the appreciably high levels of Gd that still were associated with the cells at the 5-day time point both have a very low effective r_1 and r_2.

Next we will consider the long-term fate of the Gd–chelate used in this study in the light of its thermodynamic and kinetic stability. The issue here is that both free Gd^{3+} and free chelate are toxic to cells. In addition, release of Gd^{3+} ions from the chelate might lead to considerable changes in its relaxivity properties. Gd-containing chelates preferably should have both a high thermodynamic and kinetic stability. Thermodynamic stability is an index of the intrinsic binding affinity of the Gd^{3+} ion for the chelate, while kinetic stability is a measure of the true stability of the complex under more relevant conditions, such as the presence of competing metal ions in combination with phosphate and other anions [for recent comprehensive reviews see Idee *et al.* (19,20)]. Macrocyclic chelates (such as Gd–DOTA) have a much higher thermodynamic and kinetic stability than the linear chelates (like Gd–DTPA). Among the clinically used linear chelates, Gd–DTPA–BMA (also known as Gadodiamide, or Omniscan) has the lowest thermodynamic and kinetic stability (20). Gd–DTPA–BMA is particularly relevant as the molecular structure of its Gd–DTPA complex is very much like that of the lipid-based Gd–DTPA species we used in the present study. It is important to note, however, that although both Gd–DTPA–BMA and the Gd–lipid we used are bisamides, their physicochemical properties are very different, which makes direct comparison largely impossible. When dissolved in buffer containing Zn^{2+} and phosphate, the R_1 of a suspension of liposomes containing Gd–DTPA–BSA was found to rapidly decrease (21). Based on the seminal paper by Laurent *et al.* (22), this observation was explained as being due to the Zn^{2+}-induced release of Gd^{3+} from the chelate, followed by formation of Gd^{3+}-phosphate precipitates in which the paramagnetic ion can no longer exert its T_1 shortening effect. The above transmetallation in the presence of phosphate anions has also been proposed as a likely mechanism underlying nephrogenic systemic fibrosis (NSF), a severe disorder that is predominantly associated with the use of Gd–DTPA–BMA in patients with end-stage renal disease (20). Severe renal disease is often accompanied by elevated serum levels of phosphate (23). Thakral and Abraham (24) have recently studied skin biopsies of NSF patients and have often found Gd to be associated with phosphate and calcium. Considering the above, it is plausible that (partial) release of Gd^{3+} from the DTPA chelate occurred in the intracellular compartments over a period of 5 days. Part of the endocytotic pathway involves compartments with a low pH (25), a condition known to promote Gd^{3+} release (26). The reported r_1 silencing of residual Gd^{3+} might be due to subsequent electrostatic interaction and precipitation with anions, such as phosphate. We can only speculate on the origin of the apparent absence of r_1 silencing in the case of the NT liposomes. We have evidence, however, that RGD- and NT-liposomes are internalized into different intracellular structures (see above), in which different physicochemical conditions might hold.

The origin of the r_2 silencing that we also seem to observe in the case of RGD-liposomes is less obvious. It is feasible, however, that the Gd-containing structures reach such dimensions at some stage that they enter the static dephasing regime in terms of T_2 relaxation. In this regime, the size of the relaxing structures greatly exceeds the diffusion path lengths of the water protons. In case of spin-echo based measurements of T_2 (as we used here), this implies that the contrast agent does not contribute significantly to T_2 relaxation, because of the refocusing effect of the 180° RF-pulse. In line with our observations, Anderson *et al.* (27) found that high-density endosomal labeling of mesenchymal stem cells with Gd–fullerenol, a high-relaxivity nanoparticle in which the Gd^{3+}-ion is entrapped in a cage-like structure, also led to minor T_2- and T_2^*-shortening effects.

It is important to note that we have no indications of any toxicity of the paramagnetic Gd–DTPA–BSA agent, which was used in our study [see also Kok *et al.* (10)]. However, no specific measurements were taken to exclude any such effect. Furthermore, our studies also involved a relatively short time period. Modo and co-workers (18) have recently reported a chronic one-year *in vivo* follow-up of transplanted neural stem cells, labeled with a Gd–DTPA-based low-molecular weight bimodal MRI/fluorescent contrast agent. Note that Gd–DTPA is a linear chelate with intermediate thermodynamic and kinetic stability. Despite the fact that there were no obvious signs of cell toxicity by the agent, the therapeutic efficacy of the Gd-labeled cells was negligible, whereas non-labeled stem cells led to a reduction of infarct size in a rat model of ischemic stroke. This points to a gradual degradation of the contrast agent inside the cells.

In conclusion, pre-labeling of cultured endothelial cells with paramagnetic liposomes, followed by incubation in liposome-free medium, led to dynamic changes in the effective T_1 and T_2 relaxivities of the remaining cell-associated contrast material. With time, the effective relaxivities decreased, which is possibly related with the release of Gd from the diamide-based chelate and gradual sequestration in an MR quiescent state. In order to reduce the risk of adverse effects induced by Gd release from the chelate, we have recently introduced a Gd–DOTA-based lipidic contrast agent that is immune to transmetallation under challenging *in vitro* conditions (21) and therefore also less likely to cause adverse effects when exposed to physiologically relevant

conditions. Gd–DOTA has the highest stability of all clinically approved paramagnetic contrast agents.

4. MATERIALS AND METHODS

4.1. Materials

1,2-Distearoyl-*sn*-glycero-3-phosphocholine (DSPC), cholesterol, 1,2-distearoyl-*sn*-glycero-3-phosphoethanolamine-*N*-[methoxy(-polyethyleneglycol)-2000] (PEG_{2000}-DSPE), 1,2-distearoyl-*sn*-glycero-3-phosphoethanolamine-*N*-[maleimide(polyethyleneglycol)-2000] (Mal-PEG_{2000}-DSPE) and 1,2-dipalmitoyl-*sn*-3-phosphoethanolamine-*N*-(lissamine rhodamine B sulfonyl) (rhodamine-PE) were obtained from Avanti Polar Lipids (Alabaster, AL, USA). Gd–diethylenetriaminepentaacetic acid–bis(stearylamide) (Gd–DTPA–BSA) was purchased from Gateway Chemical Technology (St Louis, MO, USA). Endothelial growth medium-2 (EGM-2) and human umbilical vein derived endothelial cells (HUVECs) were ordered with Lonza Bioscience (Switzerland). Monoclonal mouse anti-human CD31 antibody was obtained from Dakocytomation (Glostrup, Denmark). Polyclonal rabbit anti-$\alpha_v\beta_3$ integrin primary antibody was purchased from Millipore (Billerica, MA, USA). DAPI, Alexa Fluor 488 conjugated goat anti-mouse secondary antibody and Alexa Fluor 488 conjugated goat anti-rabbit secondary antibody were from Molecular Probes Europe BV (Leiden, The Netherlands). Cyclic RGD {c[RGDf(-S-acetylthioacetyl)K]} was synthesized by Ansynth Service BV (Roosendaal, The Netherlands). All other chemicals were obtained from Sigma (St Louis, MO, USA) and were of analytical grade or the best grade available.

4.2. Liposome preparation and characterization

Liposomes of 200 nm diameter containing Gd–DTPA–BSA, DSPC, cholesterol, PEG_{2000}-DSPE and Mal-PEG_{2000}-DSPE at a molar ratio of 0.75:1.10:1:0.075:0.075 were produced by lipid film hydration and extrusion according to Mulder *et al*. (28). In short, the lipids were dissolved in a 1:5 methanol:chloroform mixture. As a fluorescent marker, 0.1 mol% of rhodamine-PE was added. A lipid film was created by evaporating the chloroform–methanol mixture, using a Rotavapor R-200 (Buchi, Flawil, Switzerland). Then the lipid film was hydrated at 67°C using a HEPES buffered saline solution (HBS), containing 20 mM HEPES and 135 mM NaCl (pH 6.7). The lipid suspension was extruded at 67°C, twice, through a single 200 nm polycarbonate membrane (Whatman, Kent, UK) and six times through a double 200 nm polycarbonate membrane. After extrusion, half of the liposome suspension was modified with a RGD-peptide (6 μg μmol^{-1} total lipid) to target the $\alpha_v\beta_3$-integrin. The RGD-peptide was deacetylated and coupled to the distal end of Mal-PEG2000-DSPE. After incubation overnight, at 4°C, both batches of liposomes were centrifuged at 310 000g for 45 min. Centrifugation was used, in case of RGD-liposomes, to remove unconjugated RGD-peptide. The pellets were resuspended in HBS, pH 7.4. Lipid concentration was measured by phosphate determination according to Rouser *et al*. (29). Size and size-distribution of the liposomes were determined using dynamic light scattering (DLS; Zetasizer Nano, Malvern, UK) at 25°C. The gadolinium concentration was determined using inductively coupled plasma atomic emission spectroscopy (ICP-AES) by Philips Research (Eindhoven, The Netherlands). Both the longitudinal and transverse relaxivity were determined (6.3 T, 20°C) by fitting R_1 ($1/T_1$) and R_2 ($1/T_2$) values as a function of the gadolinium concentration of the liposome suspension using the least squares method. In this paper we refer to liposomes that were conjugated with RGD as RGD-liposomes. Non-targeted liposomes that were not conjugated with a targeting ligand will be referred to as NT-liposomes.

4.3. Cell culture

Human umbilical vein derived endothelial cells were used in all experiments. Cells were stored in liquid nitrogen upon arrival. Before use, the cells were quickly thawed in a water bath ($T = 37$°C) and divided over two gelatin-coated T75 TCPS flasks (VWR, West Chester, PA, USA). Cells were cultured in a humidified incubator at 37°C with 5% CO_2. The EGM-2 medium was replaced every 2–3 days. Cells were cultured according to procedures provided by the supplier. For the experiments, HUVECs were grown to 100% confluency and immediately used thereafter.

4.4. Experimental setup

Cells of passage 3 or 4 was used for all experiments at 100% confluency. Incubation was carried out on both gelatin-coated coverslips, for CLSM analysis, and in gelatin-coated T75 TCPS culture flasks, for MRI, FACS and ICP-AES analysis. All measurements were done in triplicate for both types of liposomes and each incubation time. To start the experiment, HUVECs were initially loaded with contrast agent by incubating them with either RGD- or NT-liposomes for 24 h using medium containing 1 μmol total lipid per milliliter. A 4 ml aliquot of liposome-containing medium was added to each T75 gelatin-coated TCPS flask and 0.5 ml of medium was added to each gelatin-coated coverslip. After the initial 24 h liposome incubation, the contrast agent-containing medium was aspirated and the cells were washed three times to remove non-adherent liposomes. Thereafter 20 and 2.5 ml of fresh medium was supplied to each T75 TCPS culture flask and gelatin coated coverslip, respectively. Samples were collected after up to 120 h of incubation with fresh medium. After incubation, the cells were washed twice with 5 ml pre-warmed (37°C) HEPES-buffered saline solution. After these washing steps, the cells grown on coverslips were fixed using 4% PFA for 15 min at room temperature. Cells in culture flasks were detached using 2 ml medium containing 0.25% trypsin and 1 mM EDTA · 4Na (Lonza Bioscience, Switzerland). The trypsin solution was neutralized using 4 ml trypsin neutralizing solution (Lonza Bioscience, Basel, Switzerland). Cells were spun down at 220g, the supernatant was removed and the cell pellet was resuspended in 200 μl 4% paraformaldehyde solution in PBS and transferred to a 300 μl Eppendorf cup. A loosely packed cell pellet was allowed to form by 4 days of storage in the dark at 4°C. Remaining cells were resuspended in 300 μl of PBS and used as cell suspension for FACS analysis (BD FACSCanto, BD Bioscience, Franklin Lakes, NJ, USA).

4.5. Magnetic resonance imaging of cell pellets

The T_1 and T_2 relaxation times and the volume of the pellets were measured using a 6.3 T horizontal bore animal MR scanner (Bruker, Ettlingen, Germany). All measurements were carried out at room temperature. Longitudinal and transverse relaxation times were measured in a 3 cm-diameter send and receive quadrature-driven birdcage coil (Rapid Biomedical, Rimpar, Germany). The Eppendorf tubes containing the loosely packed cell pellets were placed in a custom-made holder (four tubes at a time) that was filled with HEPES buffered saline solution to

facilitate shimming. T_1 was measured using a fast inversion recovery segmented FLASH sequence with: $TE = 1.5$ ms, $TR = 3.0$ ms, $\alpha = 60^\circ$, inversion time (TI) = 67–4800 ms in 80 steps, FOV = 3×3 cm^2, matrix = 128×128, slice thickness = 0.75 mm and NA = 2. The overall repetition time was 20 s. T_2 was measured using a multi-spin-echo sequence with: $TE = 9$–288 ms in 32 steps, $TR = 1000$ ms, FOV = 3.0×2.2 cm^2, matrix = 128×128, slice thickness = 0.75 mm, and NA = 4. From the images a T_1- or T_2-map was calculated using Mathematica (Wolfram Research Inc., Champaign, IL, USA). T_1 and T_2 of the different cell pellets were determined by selecting a region-of-interest within the pellet. The volume of the cell pellet was determined for each sample separately in a 0.7 cm-diameter solenoidal coil, using a 3D FLASH sequence with: $TE = 3.2$ ms, $TR = 25$ ms, $\alpha = 30^\circ$, FOV = $1.6 \times 1.6 \times 1.6$ cm^3, matrix = $128 \times 128 \times 128$, and NA = 1. Pellet volume was determined by manually setting threshold values to select the voxels inside the pellet. The segmented voxels were multiplied by the voxel volume to obtain the total volume of the pellet. The concentration of gadolinium in each cell pellet was determined by dividing the Gd content as determined by ICP-AES by the pellet volume.

4.6. Immunofluorescence

After fixation, the coverslips with HUVECs incubated with liposomes were stained using a mouse anti-human CD31 antibody to visualize the cell membrane. The cells were rinsed for 5 min with PBS followed by 60 min of incubation with the primary mouse anti-human CD31 antibody (1:40 dilution). Subsequently the cells were washed for 3×5 min with PBS followed by 30 min of incubation with a secondary Alexa Fluor 488 goat anti-mouse IgG antibody (1:200 dilution). The cells were washed for 3×5 min with PBS and the nuclei were stained for 5 min with DAPI. After staining of the nuclei the cells were rinsed for 3×5 min with PBS and subsequently mounted on a microscopy slide using Mowiol Mounting Medium. For staining of the $\alpha_v\beta_3$-integrin, first a 15 min blocking step was used, consisting of incubation with 5% (v/v) rabbit serum in PBS, which was followed by incubation with the primary mouse anti-$\alpha_v\beta_3$ integrin antibody (1:50 dilution) for 60 min. Next, the cells were rinsed for 3×5 min with PBS and subsequently incubated with Alexa Fluor 488 goat anti-mouse IgG antibody (dilution 1:200) for 1 h. Then cells were washed for 3×5 min with PBS and the nuclei were stained for 5 min with DAPI. After staining of the nuclei, the cells were rinsed for 3×5 min. with PBS and subsequently mounted on a microscopy slide using Mowiol Mounting Medium.

4.7. Confocal laser scanning microscopy

Confocal fluorescence images were recorded at room temperature on a Zeiss LSM 510 META system using a Plan-Apochromat® $63\times$/1.4 NA oil-immersion objective. Alexa Fluor 488 and rhodamine-PE were excited using the 488 and 543 nm line of a HeNe laser, respectively. The fluorescence emission of Alexa Fluor 488 and Lysotracker green were recorded with photomultiplier tubes (Hamamatsu R6357) after spectral filtering with a NFT 490 nm beamsplitter followed by a 500–550 nm bandpass filter. Rhodamine-PE emission was analyzed using the Zeiss Meta System in a wavelength range of 586–704 nm. DAPI staining of nuclei was visualized by two-photon excitation fluorescence microscopy, using the same Zeiss LSM 510 system. Excitation at 780 nm was provided by a pulsed Ti:Sapphire laser (Chameleon™; Coherent, Santa Clara, CA, USA), and fluorescence emission was detected with a 395–465 nm bandpass filter. All experiments were combined in multitrack mode and acquired confocally.

Acknowledgements

The authors gratefully acknowledge Dr Jean-Marc Idée (Guerbet) for insightful discussions and critical reading of the manuscript. This study was funded in part by the BSIK program entitled Molecular Imaging of Ischemic Heart Disease (project number BSIK03033), the Integrated EU Project MEDITRANS (FP6-2004-NMP-NI-4/IP 026668-2) and the EC-FP6-project DiMI, LSHB-CT-2005-512146. This study was performed in the framework of the European Cooperation in the field of Scientific and Technical Research (COST) D38 Action Metal-Based Systems for Molecular Imaging Applications. The authors would like to thank Jeannette Smulders (Philips Research, Eindhoven) for the ICP-MS analysis.

References

1. Hoffman JM, Gambhir SS. Molecular imaging: the vision and opportunity for radiology in the future. Radiology 2007; 244(1): 39–47.
2. Kang JH, Chung JK. Molecular-genetic imaging based on reporter gene expression. J Nucl Med 2008; 49 (Suppl 2): 164S–179S.
3. Aime S, Castelli DD, Crich SG, Gianolio E, Terreno E. Pushing the sensitivity envelope of lanthanide-based magnetic resonance imaging (MRI) contrast agents for molecular imaging applications. Acc Chem Res 2009; 42(7): 822–831.
4. Mulder WJ, Strijkers GJ, van Tilborg GA, Griffioen AW, Nicolay K. Lipid-based nanoparticles for contrast-enhanced MRI and molecular imaging. NMR Biomed 2006; 19(1): 142–164.
5. Mulder WJ, Strijkers GJ, van Tilborg GA, Cormode DP, Fayad ZA, Nicolay K. Nanoparticulate assemblies of amphiphiles and diagnostically active materials for multimodality imaging. Acc Chem Res 2009; 42(7): 904–914.
6. Bae KH, Kim YB, Lee Y, Hwang J, Park H, Park TG. Bioinspired synthesis and characterization of gadolinium-labeled magnetite nanoparticles for dual contrast T_1- and T_2-weighted magnetic resonance imaging. Bioconjugate Chem 2010; 21(3): 505–512.
7. Strijkers GJ, Mulder WJM, van Heeswijk RB, Frederik PM, Bomans P, Magusin PCMM, Nicolay K. Relaxivity of liposomal paramagnetic MRI contrast agents. Magn Reson Mater Phys 2005; 18(4): 186–192.
8. Meyer A, Auernheimer J, Modlinger A, Kessler H. Targeting RGD recognizing integrins: drug development, biomaterial research, tumor imaging and targeting. Curr Pharm Des 2006; 12(22): 2723–2747.
9. Sipkins DA, Cheresh DA, Kazemi MR, Nevin LM, Bednarski MD, Li KC. Detection of tumor angiogenesis in vivo by alphaVbeta3-targeted magnetic resonance imaging. Nat Med 1998; 4(5): 623–626.
10. Kok MB, Hak S, Mulder WJM, Van der Schaft DWJ, Strijkers GJ, Nicolay K. Cellular compartmentalization of internalized paramagnetic liposomes strongly influences both T_1 and T_2 relaxivity. Magn Reson Med 2009; 61(5): 1022–1032.
11. De Deyne PG, O'Neill A, Resneck WG, Dmytrenko GM, Pumplin DW, Bloch RJ. The vitronectin receptor associates with clathrin-coated membrane domains via the cytoplasmic domain of its beta5 subunit. J Cell Sci 1998; 111(Pt 18): 2729–2740.
12. Alam MR, Dixit V, Kang H, Li ZB, Chen X, Trejo J, Fisher M, Juliano RL. Intracellular delivery of an anionic antisense oligonucleotide via receptor-mediated endocytosis. Nucl Acids Res 2008; 36(8): 2764–2776.
13. Strijkers GJ, Hak S, Kok MB, Springer CS Jr, Nicolay K. Three-compartment T_1 relaxation model for intracellular paramagnetic contrast agents. Magn Reson Med 2009; 61(5): 1049–1058.
14. Rogers WJ, Meyer CH, Kramer CM. Technology insight: in vivo cell tracking by use of MRI. Nat Clin Pract Cardiovasc Med 2006; 3(10): 554.

15. Shyu WC, Chen CP, Lin SZ, Lee YJ, Li H. Efficient tracking of non-iron-labeled mesenchymal stem cells with serial MRI in chronic stroke rats. Stroke 2007; 38(2): 367–374.
16. Modo M, Mellodew K, Cash D, Fraser SE, Meade TJ, Price J, Williams SC. Mapping transplanted stem cell migration after a stroke: a serial, in vivo magnetic resonance imaging study. Neuroimage 2004; 21(1): 311–317.
17. Brekke C, Williams SC, Price J, Thorsen F, Modo M. Cellular multiparametric MRI of neural stem cell therapy in a rat glioma model. Neuroimage 2007; 37(3): 769–782.
18. Modo M, Beech JS, Meade TJ, Williams SC, Price J. A chronic 1 year assessment of MRI contrast agent-labelled neural stem cell transplants in stroke. Neuroimage 2009; 47 (Suppl 2): T133–142.
19. Idee JM, Port M, Robic C, Medina C, Sabatou M, Corot C. Role of thermodynamic and kinetic parameters in gadolinium chelate stability. J Magn Reson Imag 2009; 30(6): 1249–1258.
20. Idee JM, Port M, Dencausse A, Lancelot E, Corot C. Involvement of gadolinium chelates in the mechanism of nephrogenic systemic fibrosis: an update. Radiol Clin N Am 2009; 47(5): 855–869, vii.
21. Hak S, Sanders HM, Agrawal P, Langereis S, Grull H, Keizer HM, Arena F, Terreno E, Strijkers GJ, Nicolay K. A high relaxivity Gd(III)DOTA-DSPE-based liposomal contrast agent for magnetic resonance imaging. Eur J Pharm Biopharm 2009; 72(2): 397–404.
22. Laurent S, Elst LV, Copoix F, Muller RN. Stability of MRI paramagnetic contrast media: a proton relaxometric protocol for transmetallation assessment. Invest Radiol 2001; 36(2): 115–122.
23. Frenzel T, Lengsfeld P, Schirmer H, Hutter J, Weinmann HJ. Stability of gadolinium-based magnetic resonance imaging contrast agents in human serum at 37 degrees C. Invest Radiol 2008; 43(12): 817–828.
24. Thakral C, Abraham JL. Gadolinium-induced nephrogenic systemic fibrosis is associated with insoluble Gd deposits in tissues: in vivo transmetallation confirmed by microanalysis. J Cutan Pathol 2009; 36(12): 1244–1254.
25. Ohkuma S, Poole B. Fluorescence probe measurement of the intralysosomal pH in living cells and the perturbation of pH by various agents. Proc Natl Acad Sci USA 1978; 75(7): 3327–3331.
26. Wedeking P, Sotak CH, Telser J, Kumar K, Chang CA, Tweedle MF. Quantitative dependence of MR signal intensity on tissue concentration of Gd(HP-DO3A) in the nephrectomized rat. Magn Reson Imag 1992; 10(1): 97–108.
27. Anderson SA, Lee KK, Frank JA. Gadolinium-fullerenol as a paramagnetic contrast agent for cellular imaging. Invest Radiol 2006; 41(3): 332–338.
28. Mulder WJ, Strijkers GJ, Griffioen AW, van Bloois L, Molema G, Storm G, Koning GA, Nicolay K. A liposomal system for contrast-enhanced magnetic resonance imaging of molecular targets. Bioconjug Chem 2004; 15(4): 799–806.
29. Rouser G, Fkeischer S, Yamamoto A. Two dimensional thin layer chromatographic separation of polar lipids and determination of phospholipids by phosphorus analysis of spots. Lipids 1970; 5(5): 494–496.